High frequency microphone measurements for transition detection on airfoils

Døssing, Mads

Publication date:
2008

Document Version
Publisher's PDF, also known as Version of record

RISØ

Risø-R-Report

High Frequency Microphone Measurements for Transition Detection on Airfoils

Mads Døssing

Risø–R–1645(EN)

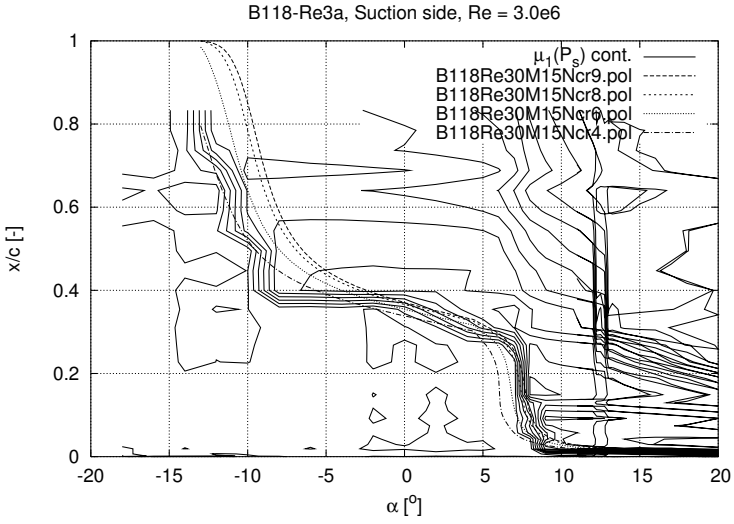

Risø National Laboratory
Technical University of Denmark
Roskilde, Denmark
June 2008

DTU

Author: Mads Døssing

Title: High Frequency Microphone Measurements for Transition Detection on Airfoils

Department: Aeroelastic Design - Wind Energy Department

Risø–R–1645(EN)
June 2008

Abstract:

Time series of pressure fluctuations has been obtained using high frequency microphones distributed over the surface of airfoils undergoing wind tunnel tests in the LM Windtunnel, owned by 'LM Glasfiber', Denmark. The present report describes the dataanalysis, with special attention given to transition detection. It is argued that the transition point can be detected by observing the increase in the mean of the Fourier spectre and that this method is very stable from a numerical point of view. Other important issues are also discussed, e.g. the variation of pressure standard deviations (sound pressure) and Tollmien-Schlichting frequencies.

The tests were made at Reynolds and Mach numbers corresponding to the operating conditions of a typical horizontal axis wind turbine (HAWT). The Risø B1-18, Risø C2-18 and NACA0015 profiles were tested and the measured transition points are reported.

ISSN 0106-2840

ISBN 978-87-550-3674-1

Contract no.:
ENS 033001/33033-0055

Group's own reg. no.:
1110060-04

Cover:
The transition to turbulence, detected using Fourier spectra data for a clean Risø B1-18 profile, is compared to XFoil results

Information Service Department
Risø National Laboratory
Technical University of Denmark
P.O.Box 49
DK-4000 Roskilde
Denmark
Telephone +45 4677 4004
bibl@risoe.dk
Fax +45 4677 4013
www.risoe.dk

Contents

List of symbols

T	Sampling time [s]
N	# samples [-]
F	Sampling frequency [Hz]
$\mathbf{Y}$	Sample vector [Pa]
$\bar{Y}$	Sample mean [Pa]
σ	Sample standard deviation [Pa]
α	Angle of attack [deg]
x	Chordwise position [m]
Re	$\frac{cU}{\nu}$ Reynolds number [-]
P_s	Power spectrum of $\mathbf{Y}$ [Pa]
K	Fourier window size [-]
f_1, f_2	High and lower bound of filtered σ [Hz]
μ_n	Statistical moments of P_s of order n [Hz]
x	Chordwise coordinate (positive from leading edge to trailing edge) [m]
z	Spanwise coordinate [m]
x_{tr}	Transition point [m]
c	Chord length [m]
$0.5\rho U^2$	Dynamic pressure [Pa]
f_{TS}	Tolmien-Schlichting frequency [Hz]
ω	Tolmien-Schlichting frequency [rad/s]
U	Incoming velocity (in windtunnel) [m/s]
δ^*	Displacement thickness [m]
U_0	Tangential velocity at distance δ^* from profile [m/s]
ν	Kinematic viscosity [m^2/s]

1 Introduction

This report describes high frequency microphone measurements on aerofoil profiles used on horizontal axis wind turbines (HAWT) and discusses the results. The measurements was made in 2007 on the NACA0015, Risø B1-18 and C2-18, in the LM windtunnel owned by 'LM Glasfiber' in Lunderskov, Denmark. The Reynolds numbers ranges from 1.6e6 to 6.0e6 corresponding to Mach numbers in the range 0.08 to 0.30.

The microphones are build into the structure on the suction and pressure side of the airfoils, thereby causing minimum disturbance to the flow. Time series of pressure fluctuations at different positions are then recorded simultaneously, enabling the variation of properties over the profile to be studied. The angle of attack, freestream velocity and turbulence intensity has been varied and different kinds of boundary layer control devices has been used (ZZ tape, leading

edge roughness (LER), trip wire/bump tape). A large amount of data has therefore been obtained and analysed. A comprehensive set of results is found in references [1], [2] and [3]. In this report the data process is described and general results are presented.

The detection of transition from laminar to turbulent flow in the boundary layer is important and various statistical quantities of the pressure fluctuations and their Fourier spectra has been examined in order to define a suitable method. The transition to turbulence is associated with a large increase in the standard deviation of the pressure fluctuations and this fact has been used to detect the transition succesfully in many cases. Unfortunately there is a number of downsides to this method. Among others, in many cases the transition is not represented by a signifant peak or sudden increase in the standard deviation and a stable numerical detection of transition is not easily defined.
The Fourier spectrum of the pressure fluctuations contains a relative large amount of high frequencies in a turbulent flow but not in a laminar flow, where background noice and freestream turbulence are dominating. Further, the onset of instabillity appears at the Tollmien-Schlichting frequency and this appears as a peak in the spectrum. The Fourier spectrum therefore contains important information regarding the nature of the boundary layer. A numerical method based on detection of the increase of the mean of the Fourier spectra at transition has proven succesfull and has allowed a vast amount of data to be analyzed automatically. The maximum derivative is detected and therefore the transition in progress. This can happen over a substantial part of the chord and this must be kept in mind when examining the results. The onset of instability can be detected manually by observing the Tollmien-Schlicting waves and the first significant change in the spectra. However, this is not easily done automatically and has not been succesfully implemented.

At Risø DTU Wind Energy Department, profile design for horizontal axis wind turbines is ongoing, and the experimental determined transition points are important for validation of the aerodynamic models used in the design process, where the calculated transition point is a crucial parameter. In the sommer of 2008 high frequency microphones will be mounted on a full size turbine to further investigate the 3D flow over real blades. It is known that 3D effects can cause transition nearer to the leading edge than in a 2D flow at the same Reynolds number and angle of attack. Microphone measurements will provide data for validation of numerial models predicting this effect. It is believed that the same methods of data analysis and transition detection as described in this report can be used in the 3D case.

The numerical data process is descriped mathematically in section 3 and the method for transition detection is written in detail. Section 2 describes the experimental setup and in section 4 the results are discussed. Some general observations regarding an effective and stable numerical analysis is also given. Qualitative results are given in section 5.

2 Experimental setup

The LM windtunnel owned by 'LM Glasfiber' in Lunderskov, Denmark is used. 3 different airfoils has been tested: Risø B1-18, Risø C2-18 and NACA-0015.

High frequency microphones are distributed over the suction and pressure side mainly in the chordwise direction. Figure 1 illustrates this, notice that the microphones are also displaced in the spanwise direction in order to avoid disturbances from upstream microphones, see Figure 2. At some chordwise positions the microphones are distributed mainly in the spanwise direction, this is seen in Figure 2. Data from these microphones can be used to study spanwise variations but in this report focus is on the chordwise distributed microphones.

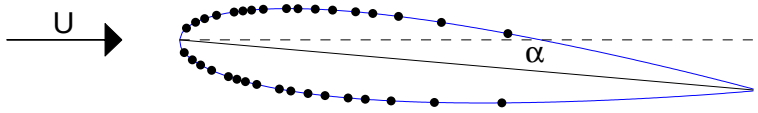

Figure 1: Microphone positions on suction (upper) and pressure (lower) side of a NACA-0015 airfoil

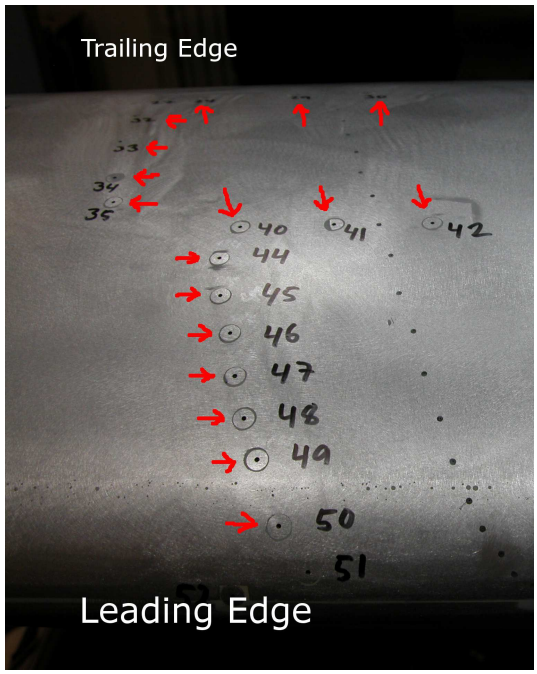

Figure 2: Example of spanwise and chordwise distribution of microphones (airfoil is seen from leading edge, suction side)

The chordwise microphone layout for all profiles are seen in Table 1 and 2. x and z are the chordwise and spanwise coordinates respectively. c is the chordlength.

B1-18		C2-18		NACA0015	
x/c	z/c	x/c	z/c	x/c	z/c
0.0000	0.0000	0.0000	0.0000	0.0100	unknown
0.0013	0.0100	0.0013	0.0100	0.0250	unknown
0.0065	0.0200	0.0065	0.0200	0.0400	unknown
0.0190	0.0300	0.0190	0.0300	0.0600	unknown
0.0293	0.0349	0.0293	0.0349	0.0900	unknown
0.0422	0.0399	0.0422	0.0399	0.1050	unknown
0.0574	0.0449	0.0574	0.0449	0.1200	unknown
0.0742	0.0499	0.0742	0.0499	0.1400	unknown
0.0920	0.0549	0.0920	0.0549	0.1800	unknown
0.1106	0.0599	0.1106	0.0599	0.2000	unknown
0.1297	0.0649	0.1297	0.0649	0.2300	unknown
0.1489	0.0699	0.1489	0.0699	0.2600	unknown
0.1880	0.0799	0.1880	0.0799	0.3000	unknown
0.2277	0.0899	0.2277	0.0899	0.3300	unknown
0.2683	0.0998	0.2683	0.0998	0.3750	unknown
0.3103	0.1098	0.3103	0.1098	0.4500	unknown
0.3542	0.1198	0.3542	0.1198	0.5667	unknown
0.4000	0.0004	0.4000	0.0004		
0.4471	0.0104	0.4471	0.0104		
0.4950	0.0203	0.4950	0.0203		
0.5432	0.0303	0.5432	0.0303		
0.5916	0.0403	0.5916	0.0403		
0.6400	0.0503	0.6400	0.0503		
0.6884	0.0603	0.6884	0.0603		
0.7365	0.0703	0.7365	0.0703		
0.7848	0.0802	0.7848	0.0802		
0.8330	0.0902	0.8330	0.0902		

Table 1: Microphone positions on suction side (chordwise)

B1-18		C2-18		NACA0015	
x/c	z/c	x/c	z/c	x/c	z/c
0.0000	0.0000	0.0000	0.0000	0.0100	unknown
0.0027	-0.0135	0.0127	-0.0600	0.0250	unknown
0.0127	-0.0270	0.0389	-0.0735	0.0400	unknown
0.0389	-0.0405	0.0828	-0.0869	0.0600	unknown
0.0828	-0.0540	0.1372	-0.1004	0.0900	unknown
0.1372	-0.0674	0.1954	-0.1139	0.1050	unknown
0.1954	-0.0809	0.2534	-0.1274	0.1200	unknown
0.2534	-0.0944	0.3688	-0.1544	0.1400	unknown
0.3108	-0.1079	0.4288	-0.0372	0.1800	unknown
0.3688	-0.1214	0.4915	-0.0520	0.2000	unknown
0.4288	-0.0055	0.5564	-0.0655	0.2300	unknown
0.4915	-0.0190	0.6197	-0.0789	0.2600	unknown
0.5564	-0.0325	0.7990	-0.1194	0.3000	unknown
0.6197	-0.0460				
0.6803	-0.0594				
0.7400	-0.0729				
0.7990	-0.0864				

Table 2: Microphone positions on pressure side (chordwise)

The airfoils are tested at different Reynolds and Mach numbers, Table 3.

Re	*Ma*
1.6e6	0.08
3.0e6	0.15
4.0e6	0.20
5.0e6	0.25
6.0e6	0.30

Table 3: Inflow conditions

A number of devices has been used to alter the incoming flow and the boundary layer, Table 4.

Clean profile
ZZ90 x/c=5% on suction side x/c=10% on pressure side
LM standard LER. ZZ 2%
Trip wire. Bump tape 2%
No grid
Turbulence grid 200 mm$\times$200 mm
Turbulence grid 100 mm$\times$100 mm
Airfoil chord: 900 mm

Table 4: Physical devices

Data is sampled at 50000 Hz in 10 seconds for all microphones simultaneously. The experiment is repeated for different angles of attack and setups. The microphones has a very small response for frequencies larger than 25000 Hz and therefore a low pass filter is not used.

3 Data processing

A number of statistical quantities has been calculated and compared in order to detect transition. In the following the process of determining the standard deviation of the pressure fluctuations and fourier spectra data is described. These quantities are usefull for studies of the boundary layer and for determining the chordwise position where transition occours.

The sampling time was T=10 seconds resulting in time series for each microphone consisting of N=TF values where F=50000 Hz is the sampling frequency. This yields a sampling vector $\mathbf{Y}$ containing the discrete pressure values

$$\mathbf{Y} = \{y_1, \ldots y_n, \ldots y_N\}^T$$

The sample mean $\bar{Y}$ and standard deviation σ is

$$\bar{Y} = \frac{1}{N}\sum_{n=1}^{N} y_n \tag{1}$$

$$\sigma = \sqrt{\frac{1}{N}\sum_{n=1}^{N} (y_n - \bar{Y})^2} \tag{2}$$

$\bar{Y}$ was in all cases small compared to σ. This was expected because the microphones measures the pressure fluctuations only. σ is a measure of the total energy of the fluctuations and therefore this quantity is expected to increase when the transition to turbulent flow occours. The positions

of the microphones are known and therefore the standard deviation versus chordwise position x can be established $\sigma(x)$. Further, since experiments are carried out at different angles of attack α, this can be extended to including this dependency, i.e. $\sigma(x,\alpha)$. $\sigma(x,\alpha)$ is discrete according to the discrete values of x and α.

$\mathbf{Y}$ can be represented by a Fourier series with power spectrum P_s

$$y_n \approx \frac{1}{2}a_0 + \sum_{k=0}^{K/2}\left(a_k \cos\frac{2\pi kn}{K} + b_k \sin\frac{2\pi kn}{K}\right) \tag{3}$$

$$P_s = \sqrt{a_k^2 + b_k^2} \quad ,k \in [0, K/2] \tag{4}$$

The Fourier coefficients are calculated by dividing $\mathbf{Y}$ into overlapping windows of size K = 4096. Each window is multiplied by the Hann window function and the window-mean is subtracted. The Fourier coefficients are then calculated for each window using the
`gsl_fft_real_float_radix2_transform`
algorithm of the GNU Scientific Library (v. 1.9). Finally the mean of all sets of Fourier coefficientens is calculated, resulting in a_k and b_k of equations 3 and 4. It is assumed that aliasing is not a problem because the microphones has very little response to frequences as high as the Nyquest frequency = 25000 Hz[1]. The frequencies according to values of k are $f_k = \frac{kF}{K}$, thus $f_k \in \left[0, \frac{F}{2}\right] = [0, 25000\,\text{Hz}]$. The frequency domain is therefore resolved into intervals of Δf=12.20 Hz which is assumed sufficiently small to show any important peaks in the power spectrum.

Notice that the calculated fourier coefficients are to small because of the application of the Hann window function. However this error is systematic and as long as only qualitative properties are needed it is not relevant.

The standard deviation of a time series can be found as

$$\sigma = \sqrt{\frac{1}{2}\sum_{k=1}^{\infty}\left(a_k^2 + b_k^2\right)} \approx \sqrt{\frac{1}{2}\sum_{k=1}^{K/2}\left(a_k^2 + b_k^2\right)} \tag{5}$$

Using this result filtered standard deviations can be found. I.e. by setting a_k=b_k=0 for k-values according to selected frequencies those frequencies are not included in the calculation of the filtered standard deviation. In the following, only frequencies in the range $f \in [f_1, f_2]$ are included. Typical values are $f \in [2000, 25000]$. Because of the limited number of fourier coefficients this approximation is not accurate but does provide an easy way to examine which frequencies contributes to σ. In particular it is sometimes usefull to filter away low frequencies which in general are associated with the formation of large eddies in stall.

Important: The application of the Hahn-window function affects the results, leading to too low values of a_k, b_k and therefore also σ, if calculated using (5).

Statistical properties of the powerspectrum are calculated as raw moments of n'th order

$$\mu_n = \frac{\int (f-\mu_1)^n P_s\, df}{\int P_s\, df}$$

However, the first moment is calculated about zero

$$\mu_1 = \frac{\int f P_s\, df}{\int P_s\, df}$$

The above formulas are equivalent to treating the power spectrum as a probability density function with mean μ_1. Studies show that the maximum positive derivative of μ_1 with respect to chordwise position is a good and numerically stable indicator of the transition point. The

[1] It turns out that the microphones can in fact detect such high frequencies, but it does not influence the results significantly

higher order moments did not yield any consistent results and will not be treatet further here. In the following transition is defined as

$$x_{tr} \equiv \left\{ x \quad | \quad \left. \frac{d\mu_1}{dx} \right|_x = max\left(\frac{d\mu_1}{dx} \right) \right\}$$

Calculating a derivative by numerical means is not easy due to the fluctuations of the experimental data. Therefore the data must be smoothed using a suitable function. Figure 3 shows an example. Notice that the value of the derivative can easily be wrong by a factor of 2 or more. In many cases there is signifcant noise at the leading edge, and the result can be that the dataset is smooth'ed to much. This leads to a maximum derivative to far upstream, and therefore the transition point can in some cases not be found accurately near the leading edge. Contour plots of μ_1 avoids these problems and will clearly show what is correct.

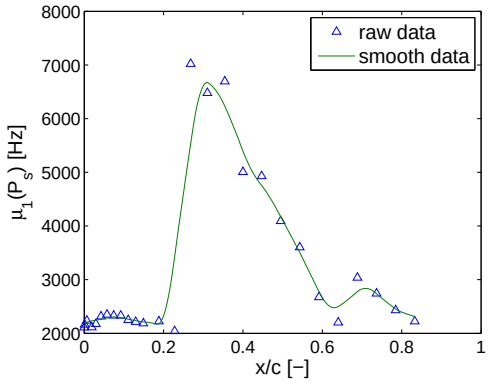

Figure 3: Example of raw and smooth data

4 Discussion

The following discussion is based on quantities calculated as described in section 3. Only quantities related to the suction side is treated but all data is available for the pressure side as well.

4.1 Correlation between standard deviations and transition point

Figure 4 shows plots of the calculated st.dev. versus chordwise position and angle of attack for a clean B1-18 profile at a Reynolds number of Re=1.6e6. There is a clear correlation between the peaks of the st.dev. σ and the transition point x_{tr}. It is also seen that σ increases substantially in stall, especially near the trailing edge where large vortices are sheed.

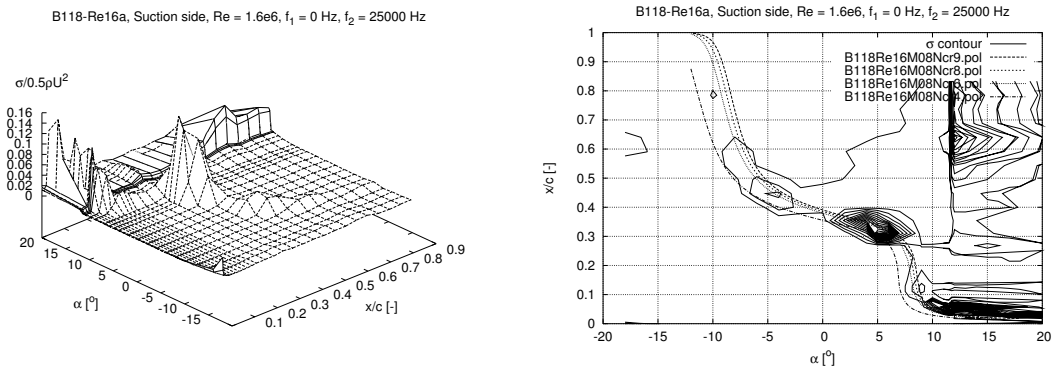

Figure 4: Left: Standard deviations. Right: Countour plot of standard deviation and transition points calculated in XFoil

The XFoil[2] data is calculated at 4 different N_{crit} values (4, 6, 8 and 9) corresponding to turbulence intencities of the incoming flow of 0.563%, 0.245%, 0.106% and 0.07% respectively. The result shown here is very good but in general the data is harder to interpret for higher Reynolds number, increasing turbulence intensity and use of ZZ90, LER etc.. Therefore, the method of subsection 4.7 is preferred.

4.2 Filtered VS unfiltered standard deviation data

Figure 5 shows the st.dev. of a clean B1-18 profile at a Reynolds number of *Re*=4.0e6, calculated with and without filtering of frequencies. The filtering produces a cleaner picture and it is clear where the low frequencies contributes significantly to σ. I.e. in the deep stall region starting a small distance from the leading edge. Notice that the values of the filtered σ are artificially lower than the unfiltered because of the Hann window as explained in section 3.

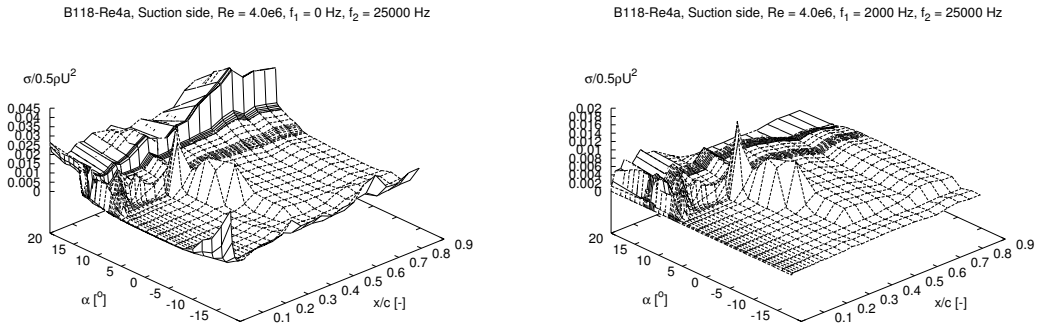

Figure 5: Left: Standard deviations without filtering. Right: Standard deviations of frequencies above 2000 Hz

4.3 The magnitude and scaling of standard deviation data

In the following clean profiles are discussed.

The standard deviation of the pressure fluctuations are scaled by the dynamic pressure, $0.5\rho U^2$

$$\frac{\sigma}{0.5\rho U^2}$$

[2] XFoil version 6.96

This quantity was comparable for all profiles for a given Reynolds number and inflow angle. In this context comparable means that the relative differences are within approximately 25% but in some cases larger. The values are strongly dependent on chordwise position and changes when trip wires etc. are used.

σ increases with Reynolds number but $\frac{\sigma}{0.5\rho U^2}$ decreases. Table 5 shows typical values in deep stall.

Re	$\frac{\sigma}{0.5\rho U^2}$
1.60e6	≈ 0.08
3.30e6	≈ 0.04
4.00e6	≈ 0.035
5.00e6	≈ 0.03
6.00e6	≈ 0.02

Table 5: Rough values of scaled pressure standard deviations in deep stall showing the decrease with *Re*

The chordwise variation is large. In deep stall the standard deviation is largest near the trailing edge, but when not in stall the standard deviation is very small in the laminar region, and larger after transition. However, not as large as in stall. Around transition there is, under certain conditions, a clear peak value. Typical values in the turbulent layer after transition for profiles not in stall are in the order

$$\frac{\sigma}{0.5\rho U^2} \approx 0.01 - 0.02$$

4.4 Fourier analysis

Figure 6 shows the powerspectra calculated at the different chordwise positions of the microphones for a B1-18 profile at *Re* = 1.6e6, α=7.0 degrees. Also seen is the signal from background microphones. The spectre contains very little energy until $x/c \approx$0.2. A little further downstream a peak appears in the spectre around a frequency of $\approx$ 1000 Hz which develops into a broad Fourier spectre a short distance downstream. The small peak is the initial instability around the Tollmien-Schlichting frequency (this is treated further in section 4.5).

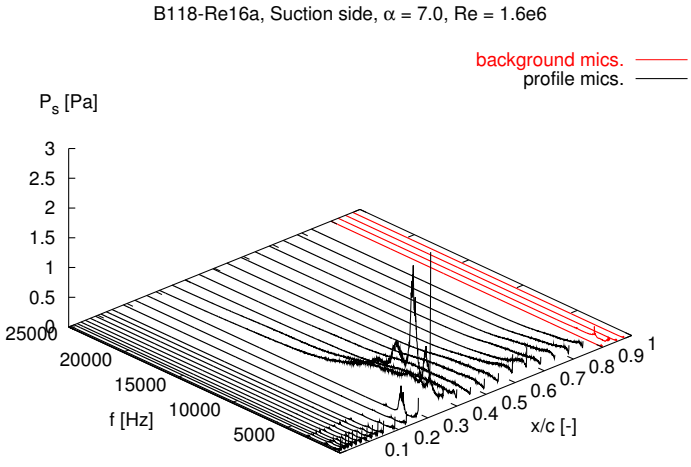

Figure 6: Power spectra versus chordwise positions for α=7.0 degrees

4.5 Tollmien-Schlichting frequencies

The Tollmien-Schlichting frequencies (f_{TS} or ω) can be read from the fourier spectre. The following results are for a clean B1-18 profile without turbulence grid. Figure 7.left shows f_{TS} at different α and *Re*. The results are reported using the following dimensionless groups[3].

$$Re_{\delta^*} = \frac{U\delta^*}{\nu} \quad , \frac{\omega\nu}{U_0^2}$$

δ^* is the displacement thickness and U_0 is the tangential velocity at the distance δ^* from the profile, both are calculated using XFoil. U and ν are the windtunnel velocity and the kinematic viscosity of air (1.50e-5m^2/s). Figure 7.right shows a plot of these groups. This shows with some succes that the data scales to comparable values (i.e. the values collapses onto a line). The numerical values are comparable with those reported in [4] page 354 for a flat plate, but are approximately 25% lower. The results of Figure 7 strongly indicates that it is in fact the Tollmien-Schlichting frequency which is observed.

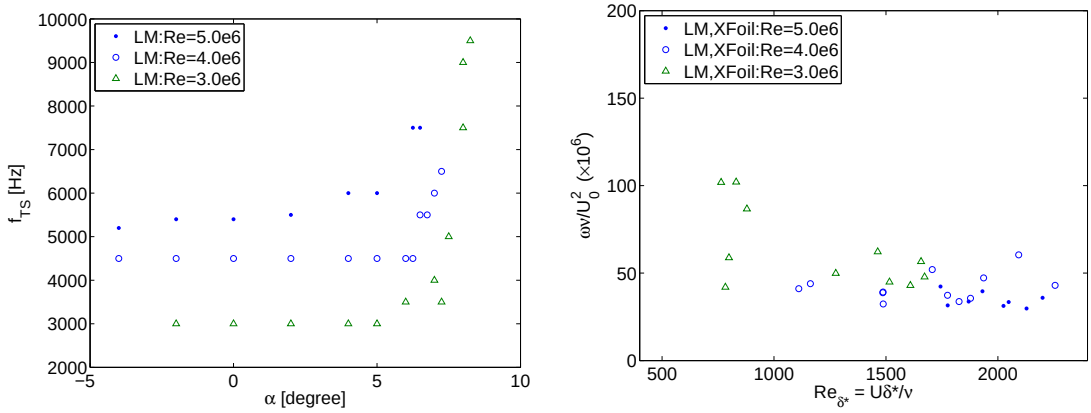

Figure 7: Left: Tollmien-Schlichting frequencies. Right: Dimensionless groups

4.6 Development of boundary layer visualized by Fourier spectra

The Fourier spectra reveals information about the changes in the boundary layer as α is increased. Figure 8 shows (in row major order) results for α=$\{4.0, 6.0, 6.5, 6.75, 8.0, 10.0\}$ degrees for a clean B1-18 profile at *Re*=5.0*e*6. Initially the boundary layer is clearly divided into a laminar and a turbulent zone. At α=6.0 disturbances occour near the leading edge which grows and eventually merges with the turbulent zone at α=10.0.

In Figure 8 it is seen that the microphones does respond to frequences as high as the Nyquist frequency, meaning that aliasing becomes a problem. Therefore, low pass filters should be used in the future. The method for transition detection described in section 4.7 is not sensitive to this.

[3] See e.g. [4]

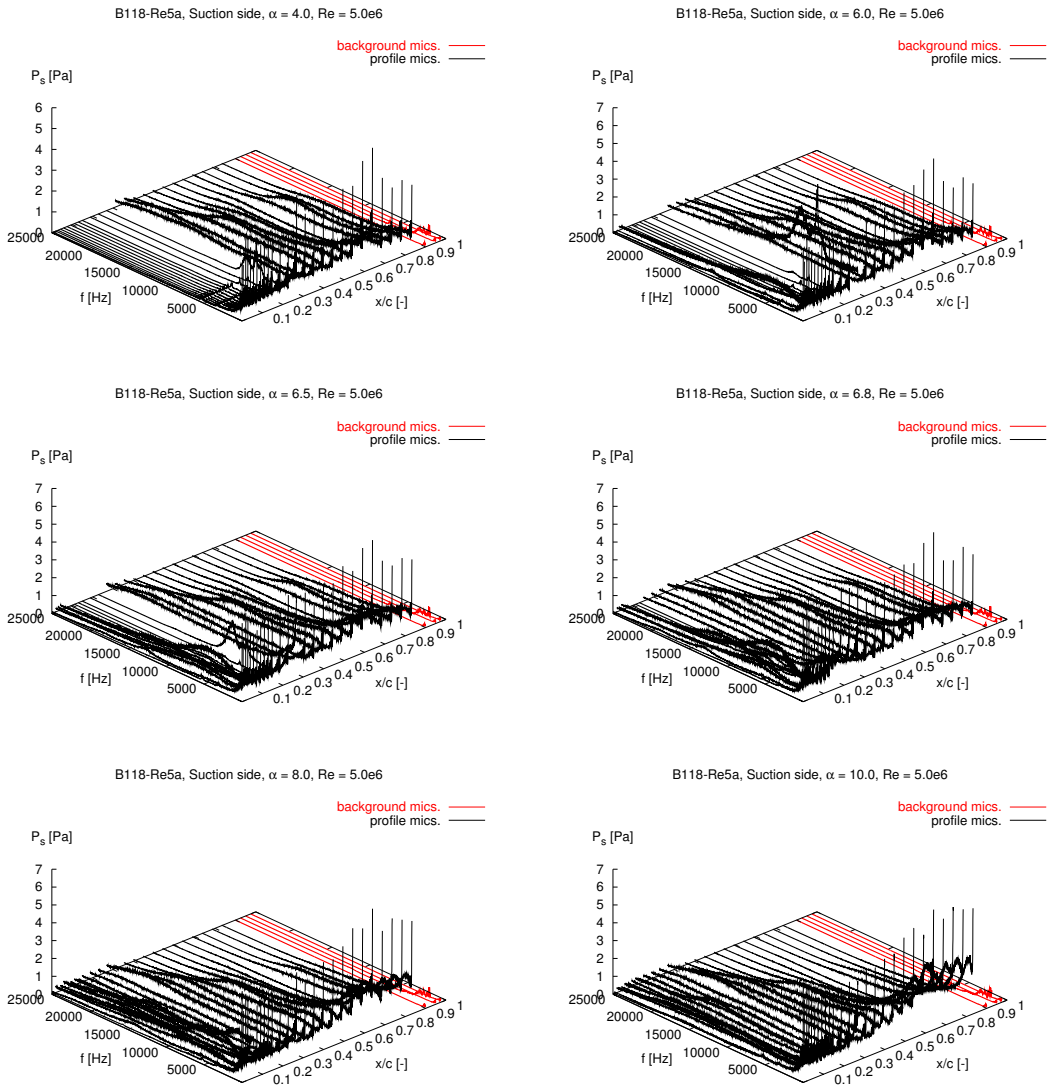

Figure 8: Fourier spectra for increasing α

4.7 Correlation between $max\left\{\frac{d\mu_1}{dx}\right\}$ and transition

Results shows a good correlation between the largest positive derivative of the mean of the Fourier spectre and the transition point and this is the method used for automatic detection. Refer to section 3 for details. Figure 9 shows μ_1 against α and x/c and the corresponding contour plot for a clean B1-18 profile at *Re*=5.0e6. There is a band of close contours indicating a high derivative and therefore transition. In this case the band is approximately 5% of the chord wide, indicating that the full transition from laminar to turbulent flow happens over 5% of the chord. Typical values are 5 to 10% but in some cases the transition occours over a larger part of the chord. This is sometimes the case when the inflow turbulence is increased which causes a transition nearer to the leading edge. At α ≈5-7 degrees there is a region at the leading edge with a high noise level, but because the transition is detected as the highest *positive* derivative it is at $x/c \approx 0.3$. However, in general it should be expected that the transition may be detected erroneously to be at the leading edge. The 3D and contour plots will clearly show what is correct.

Instability sets in at the leading edge of the band of contours, i.e. a short distance upstream of

the defined transition point. This is where the Tollmien Schlichting frequencies are observed and it is equivalent to a large second order derivative. This quantity is not easily calculated numerically and automatic detection of instability has not been attempted.

In this case XFoil fails to predict the transition accurately for $\alpha < 5$ degree, something which was also seen in other cases.

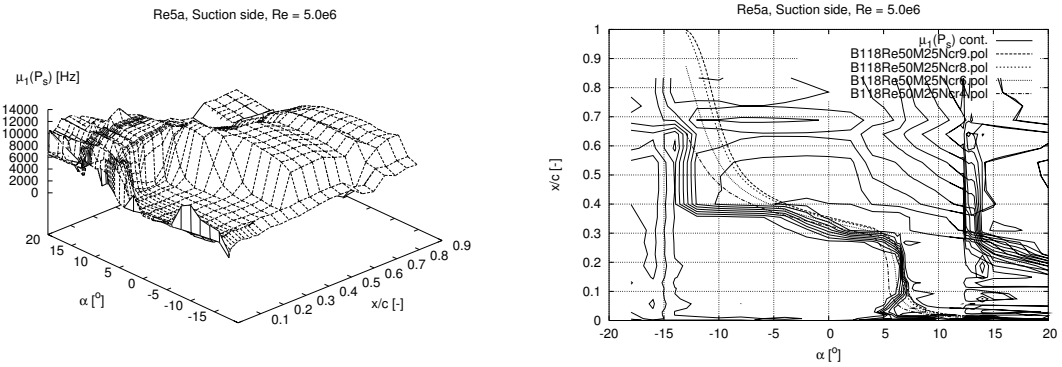

Figure 9: Left: 3D plot of $\mu_1(P_s)$. Right: Countour plot and transition points calculated in XFoil

The actual value of the derivative at the detected transition is important because a low value indicates no transition and a medium value indicates a transition over a large chordwise span. A high value indicates a sharp transition. The 3D and contour plots will clearly show what is the case. The numerically detected transition points are stored in text files (example given below) the third column is the calculated derivative. Notice that this is the derivative of the smooth data and it can have a substantial error. This author recommends that any value lower than $\approx$ 35000 is taken to indicate no transition.

```
B118-Re3a
alpha          [degrees] angle of attack
xtr*           [-]       transition point (x*=x/c) predicted by max[d(mu1(Ps))/dx*]
d(mu1)/dx*     [Hz/-]    d(mu1(Ps))/dx* evaluated at xtr* (=max[d(mu1(Ps))/dx*])
max(mu1)       [Hz]      max mu1 of all chordwise positions

alpha   xtr*    d(mu1)/dx*  max(mu1)
------  ------  ----------  --------
-18.00  0.6823     18416.4    3767.8
-16.00  0.6823     18663.5    6183.6
-14.00  0.6823     14308.4    7002.6
-12.00  0.6907     54317.7    7916.0
-10.00  0.5358     53303.7    8676.9
 -8.00  0.3558     64614.4    8907.9
 -6.00  0.3558     68653.6    9064.3
 -4.00  0.3558     68045.0    9277.7
 -2.00  0.3558     73670.8    9399.6
  0.00  0.3558     70077.4    9184.7
  2.00  0.3516     60009.1    9127.9
  4.00  0.3098     71225.2    9383.8
  5.00  0.3098     76517.2    9830.1
  6.00  0.3056     77583.3   10096.1
  7.00  0.2679     74647.0   10424.1
  8.00  0.1339     64073.3   12070.1
  9.00  0.0460    108102.8   13340.4
 10.00  0.0460    102213.7   13183.4
```

4.8 Accuracy

There is a relative large distance between the microphones and this can be expected to affect the accuracy, but this is only a serious problem if the transition point is detected by peaks in

σ. Figure 6 shows the good agreement between transition detected by peaks in σ compared to XFoil calculations for a clean B1-18 profile at Re=1.60e6 . The errorbars indicate the distance to the neighbour microphones and because any peaks between microphones can not be detected this also indicates the uncertainty. The method of section 4.7 partly overcomes this problem because μ_1 can be interpolated succesfully between microphones. The reason is that μ_1 under transition grows monotonically to an upper value of approximately 10000 Hz, and then it maintains this value or decreases slowly. Thus μ_1 behaves very well under transition. The number of microphones can be kept relatively low and the risk of flow-interaction is minimized.

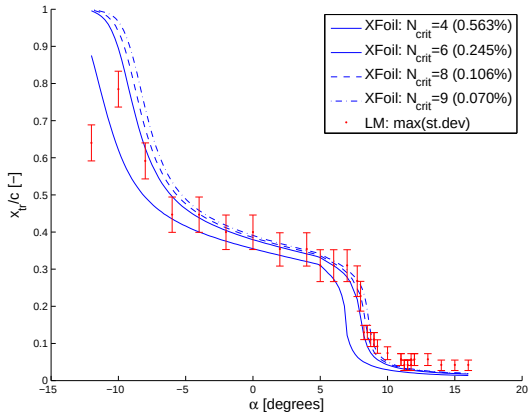

Figure 10: Transition detected by peaks in σ compared to XFoil calculations

High frequency standing waves may occour in the microphone holes, but no measurement has indicated that this is significant. I.e. there is no peak in the spectra which is repeated in measurements.

The response functions of the microphones has not been compared. This should be done in order to detect faulty microphones before doing measurements. There are indications that the microphones did not have the same gain in the NACA0015 measurements, something which can be verified by comparing microphones on the upper and lower side at zero degree angle of attack, where the response of this symmetric airfoil should be the same. Notice that μ_1 is independent of gain errors.

Numerical differentiation of μ_1 is not easy, but in this work it is made stable by the use of smoothing. The major drawback is that leading edge noise can interact with the noise related to transition, if the transition is close the leading edge. The result is that transition can not be determined accurately if within approximately 10% of the leading edge.

5 Results

In this section the autodetected transition points are presented. All results are for cases without turbulence grid.

5.1 Transition points on clean profiles

Figure 11 shows automatically detected transition points for clean profiles without turbulence grids. As mentioned earlier there is uncertainty related to the detection near the leading edge and this can be seen in the plots (i.e. the values in the range x/c=[0 0.1] are uncertain). When not near the leading edge it is seen that the transition point moves closer to the leading edge

with increasing Reynolds number and the inflow angle where the transition moves fast forward to the leading edge decreases with Reynolds number. Notice that this angle can be determined with great accuracy and that the uncertain data for higher angles is not important because the transition point is known to be very near the leading edge anyway.

The results for the NACA 0015 profile may have been affected by a cavity around certain microphones. Furthermore, the microphones were placed directly downstream of each other and upstream microphones may therefore have affected the results (i.e. by causing early transition).

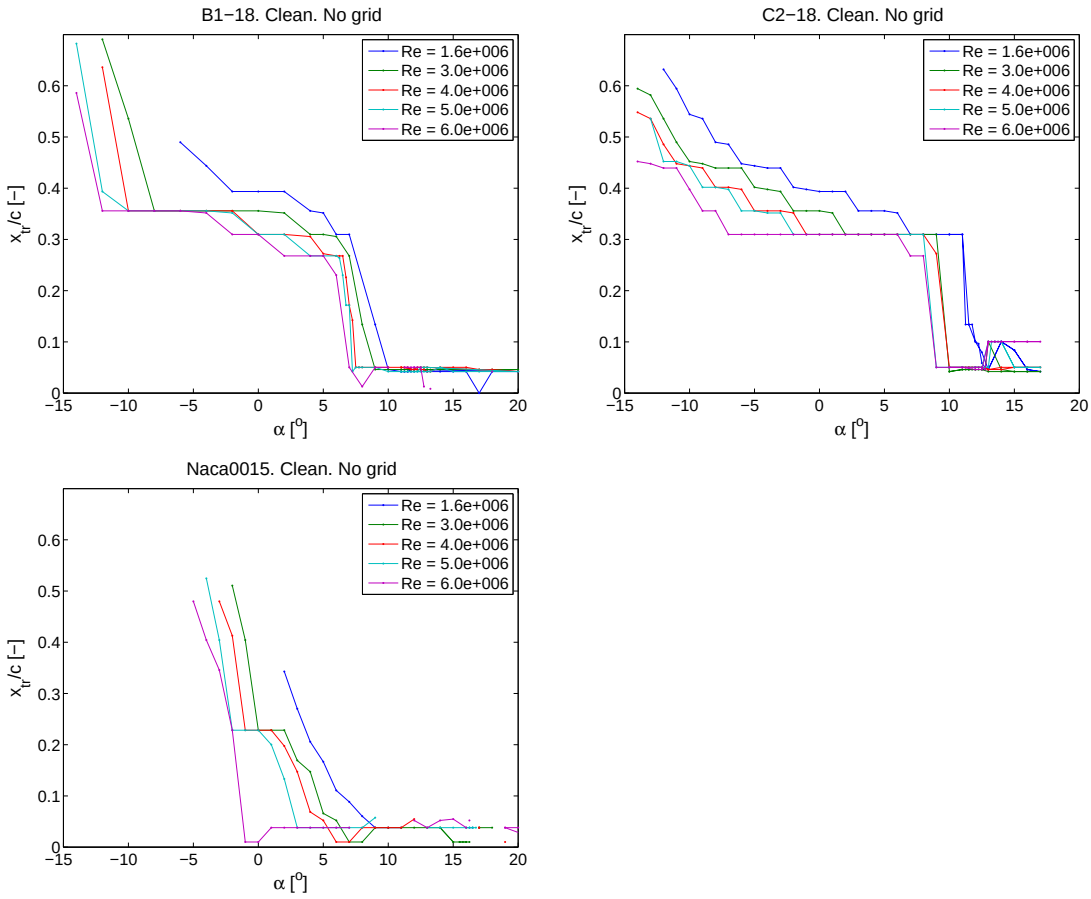

Figure 11: Transition points on clean profiles, no turbulence grids

5.2 Effect of leading edge roughness

Figure 12 shows contourplots of $\mu_1(P_s)$ for a B1-18 profile at *Re*=3.0e6 no turbulence grid, with and without leading edge roughness, respectively. It is noticed that XFoil predicts the transition well on the clean profile for $\alpha >$-2 deg. With leading edge roughness the transition occours near the leading edge for $\alpha >$-5 deg. In general, LER triggers transition even without turbulence grids (i.e. low turbulence intensity) at low Reynolds numbers. For higher Reynolds numbers the transition point stays close to the leading edge at even lower (more negative) angles of attack. Figure 13 shows the autodetected transition points.

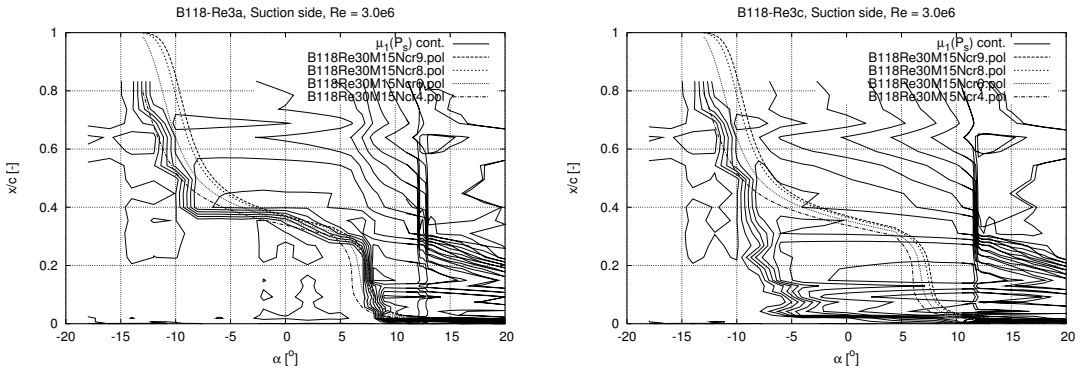

Figure 12: Left: Contour plot of μ_1, clean profile. Right: Contour plot of μ_1, with leading edge roughness (LER)

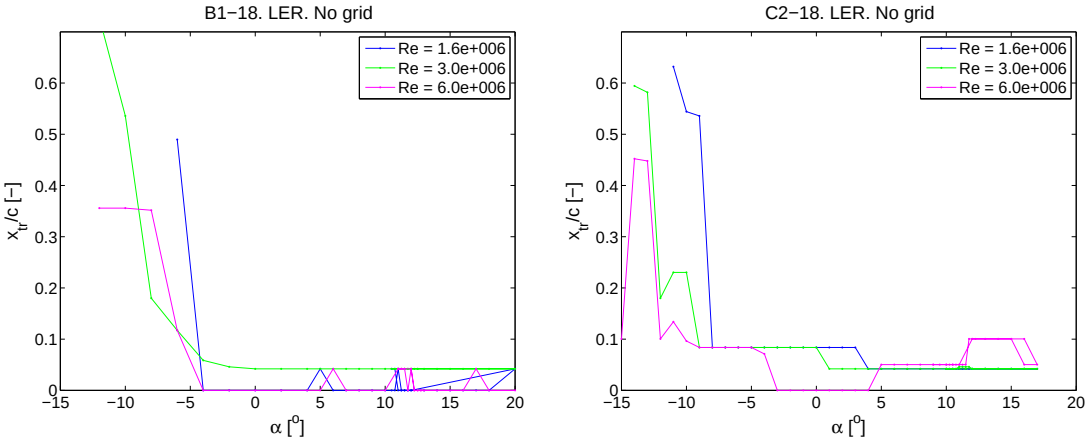

Figure 13: Transition points on profiles with leading edge roughness, no turbulence grids

5.3 Effect of trip wire

Figure 14 shows a contourplot of the same data as in section 5.2 but for a profile with trip wire/bump tape attached instead of LER. Comparing with Figure 12.left, showing the clean profile, the difference is very small. The effect is that the transition jumps to the leading edge at $\alpha \approx 6$ deg. instead of $\alpha \approx 7.5$ deg. For *Re*=1.6e6 there is no noticeable effect, but for *Re*=6.0e6 there is a large effect and the transition jumps to the leading edge at $\alpha \approx 0$ deg. instead of at $\alpha \approx 6.5$ deg. It is concluded that the effect of the trip wire depends strongly on Reynolds number. Figure 15 shows the autodetected transition points. Notice that if turbulence grids are mounted there is a noticeable effect even at *Re*=1.6e6.

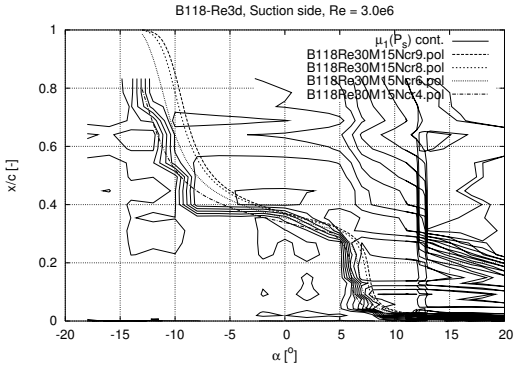

Figure 14: Contour plot of μ_1, with trip wire bump tape.

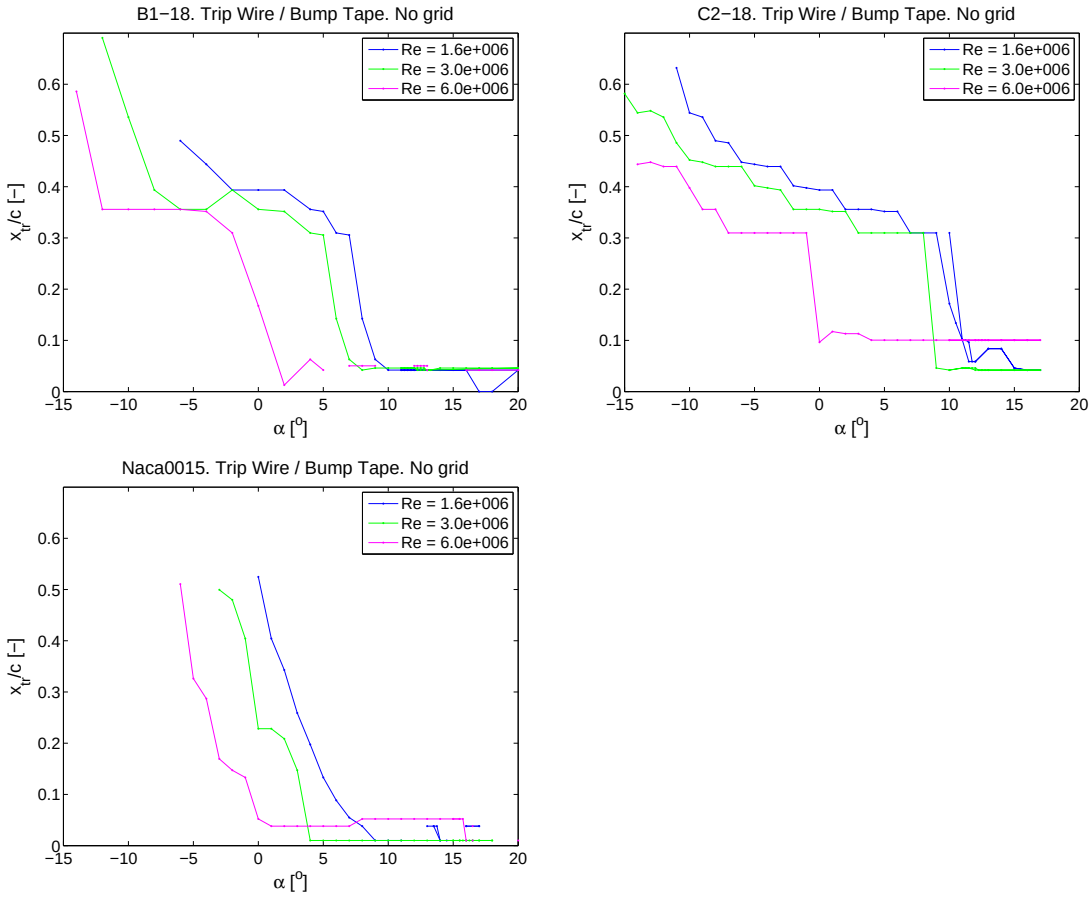

Figure 15: Transition points on profiles with trip wire, no turbulence grids

5.4 Effect of ZZ90

Figure 16 shows a contourplot of the same data as in section 5.2 but for a profile with ZZ90 attached instead of LER. The effect is the same as for the leading edge roughness (LER). Figure 17 shows the autodetected transition points.

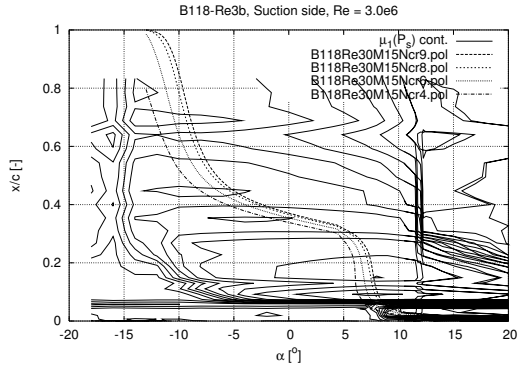

Figure 16: Contour plot of μ_1, with ZZ90

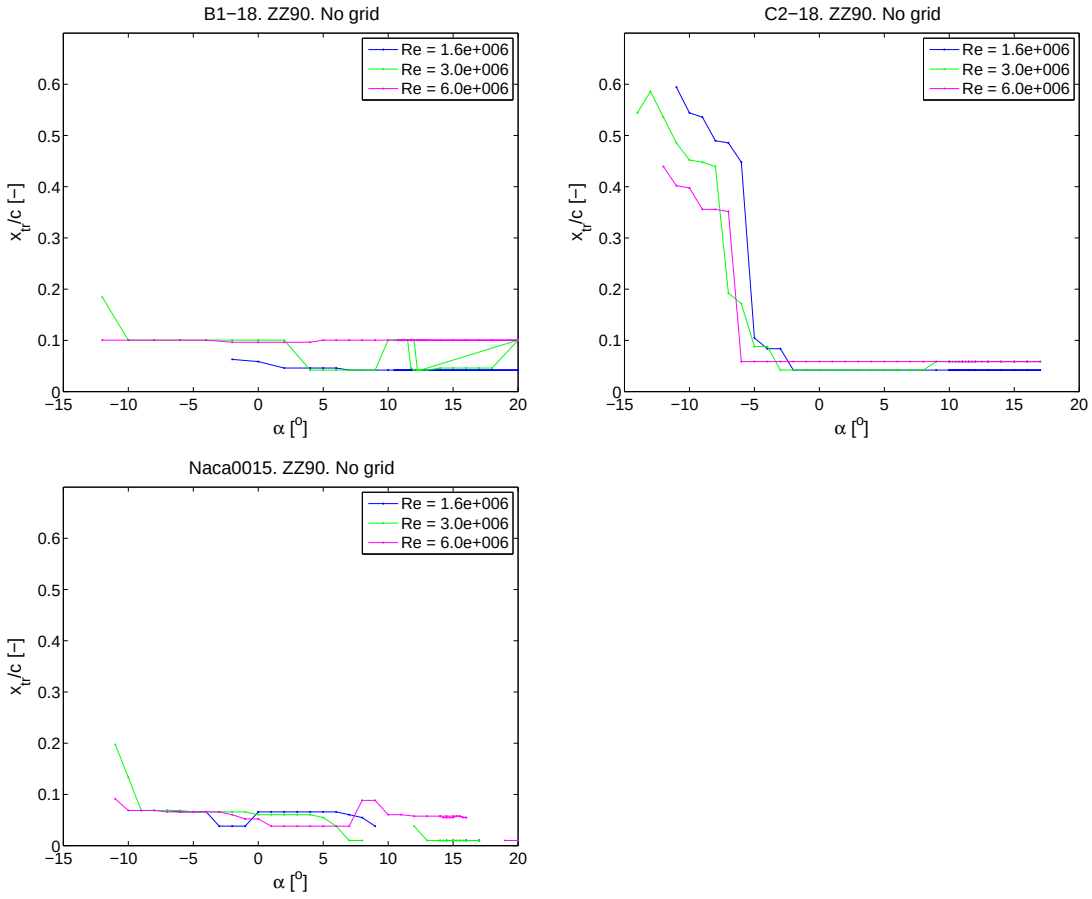

Figure 17: Transition points on profiles with ZZ90, no turbulence grids

5.5 Effect of turbulence grid

Unfortunately the turbulence intensity, with turbulence grids mounted, has not been measured succesfully. The results clearly shows that the increased turbulence forces the transition points closer to the leading edge. Refer to [1], [2] and [3] for details about specific cases.

6 Archived data

The results for a large number of experiments are given in the technical reports [1], [2] and [3]. This includes tables of the detected transition points and a number of plots showing standard deviation and Fourier transform data (μ_1). Plots of the fourier transforms themselves are not included.

The data in file format is accessible from

`\\veadbs-02\archive\MicroTunnel`

on the Risø internal net. The power spectra given by (4) are stored in binary `.tim` files. For each increasing k-value a 4 byte data-value is stored for all 80 channels according to increasing channel number. The size of the files are therefore

size = 2049 k-values $\times$ *80 channels* $\times$ *4 bytes = 655680 bytes*

Notice: When XFoil results are included in figures they correspond to the case of a clean airfoil (free transition) in most cases (but not all !). This is done in order to quickly compare the effect of e.g. leading edge roughness to the clean airfoil. Something which is possible because the XFoil results in general predicts the transition on clean airfoils well. Again, there are exceptions !

7 Conclusion

A method for determining transition on airfoils has been presented. The method is numerically stable which enables a large amount of data to be analysed efficiently and the transition to be detected automatically. Some care must be taken when using autodetected transition points. The numerical differentiation of Fourier data are in some cases not accurate near the leading edge. E.g. contour plots clearly shows a high derivative at x/c=5% but it is detected at 10%. When not near the leading edge, transition can be detected accurately even though a relatively low number of microphones are used. The method implemented detects the transition in progress wich happens over a substantial part of the chord. The initial instability is well defined and can be determed by manually inspecting data and identifying Tollmien-Schlichting frequency peaks or a large second order derivative of the Fourier spectre mean.

A large amount of data has been analysed and the transition point under various conditions has been reported for the Risø B1-18, Risø C2-18 and NACA0015 profile. For clean profiles the transition moves towards the leading edge with increasing Reynolds number.
The effect of trip wire / bump tape on the Risø profiles is strongly dependent on Reynolds number. At Re=1.60e6 they are largely unaffected but strongly affected at Re=6.0e6.
ZZ90 and leading edge roughness both triggers transition immediately.

The microphone layout on the NACA-0015 profile may have caused caused early transition in some cases !

References

[1] Døssing M. High Frequency Microphone Measurements for Transition Detection on Airfoils - Risø B1-18 Appendix Report. Risø R-report ISBN 978-87-550-3675-8, Risø DTU, Wind Energy Department, 2008.

[2] Døssing M. High Frequency Microphone Measurements for Transition Detection on Airfoils - Risø C2-18 Appendix Report. Risø R-report ISBN 978-87-550-3676-5, Risø DTU, Wind Energy Department, 2008.

[3] Døssing M. High Frequency Microphone Measurements for Transition Detection on Airfoils - NACA-0015 Appendix Report. Risø R-report ISBN 978-87-550-3677-2, Risø DTU, Wind Energy Department, 2008.

[4] Frank M. White. *Viscous Fluid Flow*, volume Second Edition. McGraw-Hill International Editions, 1991.

[5] Drela M. XFOIL: An Analysis and Design System for Low Reynolds Number Airfoils. lecture Notes in Engineering: Low Reynolds Number Aerodynamics, T.J. mueller (ed.), Springer Verlag, New York, **54**. 1989.

[6] Bak C. (ed). Forskning i Aeroelasticitet EFP-2007. Wind Energy Department, Aeroelastic Design. Risø DTU. 2007.

[7] Bove S. Fuglsang P. Wind Tunnel Testing Of Airfoils Involves More Than Just Wall Corrections. *Paper presented at EWEC 2008, Brussels*, 2008.

Risø's research is aimed at solving concrete problems in the society.

Research targets are set through continuous dialogue with business, the political system and researchers.

The effects of our research are sustainable energy supply and new technology for the health sector.